

Nanofocusing of surface plasmon polaritons by a pyramidal structure on an aperture

Kazuo Tanaka^{1*}, Kiyofumi Katayama² and Masahiro Tanaka¹

¹Department of Electronics and Computer Engineering, Gifu University, Yanagido 1-1, Gifu City, 501-1193 Japan

²Faculty of Administration and Informatics, University of Hamamatsu, Hamamatsu City, 431-2102 Japan

*tanakazu@.gifu-u.ac.jp

Abstract: A numerical study of the nanofocusing of surface plasmon polaritons (SPPs) by a pyramidal structure on a rectangular aperture is performed by the volume integral equation method. It is possible to perform nanofocusing using this structure by using a linearly polarized wave as the incident wave. The focusing process of SPPs by the tip of the pyramidal structure has been demonstrated numerically. The characteristics of the focused optical field near the tip have been investigated in detail. It was found to be similar to that of monopole rather than that of a tiny dipole. The optical field at the tip is sensitive to the local shape of the tip. The enhanced intensity on the tip increases with an increase in the aperture width.

©2009 Optical Society of America

OCIS codes: (230.7370) Waveguide; (240.6680) Surface plasmons; (260.2110) Electromagnetic theory

References and links

1. M. Ohtsu, and H. Hori, "Near-Field Nano-Optics: From Basic Principles to Nano-Fabrication and Nano-Photonics," Plenum Pub. Corp. (1999).
2. V. M. Shalaev and S. Kawata ed., "Nanophotonics with Surface Plasmons," Elsevier Science Ltd. (2007).
3. M. Ohtsu, K. Kobayashi, T. Kawazoe, T. Yatsui, and M. Naruse, "Principles of Nanophotonics," Chapman & Hall (2008).
4. J. Takahara, S. Yamagishi, H. Taki, A. Morimoto, and T. Kobayashi, "Guiding of a one-dimensional optical beam with nanometer diameter," Opt. Lett. **22**(7), 475–477 (1997).
5. S. A. Maier, M. L. Brongersma, P. G. Kik, S. Meltzer, A. A. G. Requicha, and H. A. Atwater, "Plasmonics - A route to nanoscale optical devices," Adv. Mater. **13**(19), 1501–1505 (2001).
6. W. L. Barnes, A. Dereux, and T. W. Ebbesen, "Surface plasmon subwavelength optics," Nature **424**(6950), 824–830 (2003).
7. K. Tanaka, and M. Tanaka, "Simulations of nanometric optical circuits based on surface plasmon polariton gap waveguide," Appl. Phys. Lett. **82**(8), 1158–1160 (2003).
8. S. I. Bozhevolnyi, V. S. Volkov, E. Devaux, J. Y. Laluet, and T. W. Ebbesen, "Channel plasmon subwavelength waveguide components including interferometers and ring resonators," Nature **440**(7083), 508–511 (2006).
9. S. I. Bozhevolnyi, "Plasmonic Nanowaveguide and Circuits", World Scientific, 2008.
10. E. Oesterschulze, G. Georgiev, M. Müller-Wiegand, A. Vollkopf, and O. Rudow, "Transmission line probe based on a bow-tie antenna," J. Microsc. **202**(Pt 1), 39–44 (2001).
11. S. Xiaolei, L. Hesselink, and R. L. Thornton, "Greatly enhanced power throughput from a "C"-shaped metallic nano-aperture for near field optical applications", Quantum Electronics and Laser Science Conference, 2002. Technical Digest. 40.
12. A. Naber, D. Molenda, U. C. Fischer, H.-J. Maas, C. Höppener, N. Lu, and H. Fuchs, "Enhanced light confinement in a near-field optical probe with a triangular aperture," Phys. Rev. Lett. **89**(21), 210801–210804 (2002).
13. K. Tanaka, and M. Tanaka, "Simulation of an aperture in the thick metallic screen that gives high intensity and small spot size using surface plasmon polariton," J. Microsc. **210**(Pt 3), 294–300 (2003).
14. K. V. Nerkararyan, "Superfocusing of a surface polariton in a wedge-like structure," Phys. Lett. A **237**(1-2), 103–105 (1997).
15. A. J. Babadjanyan, N. L. Margaryan, and K. V. Nerkararyan, "Superfocusing of surface polaritons in the conical structure," J. Appl. Phys. **87**(8), 3785 (2000).
16. M. I. Stockman, "Nanofocusing of optical energy in tapered plasmonic waveguides," Phys. Rev. Lett. **93**(13), 137404 (2004).
17. N. A. Janunts, K. S. Baghdasaryan, Kh. V. Nerkararyan and B. Hecht, "Excitation and superfocusing of surface plasmon polaritons on a silver-coated optical fiber tip," Opt. Comm. **253**, (2005).
18. R. Ruppin, "Effect of non-locality on nanofocusing of surface plasmon field intensity in a conical tip," Phys. Lett. A **340**(1-4), 299–302 (2005).

19. M. W. Vogel, and K. Dmitri, "Adiabatic nano-focusing of plasmons by metallic tapered rods in the presence of dissipation," *Phys. Lett. A* **363**(5-6), 507–511 (2007).
20. N. A. Issa and R. Guckenberger, "Optical nanofocusing on tapered metallic waveguides," *Plasmonics* **2**, 1557–1955 (Print) 1557–1963 (Online) (2007).
21. W. Chen, and Q. Zhan, "Numerical study of an apertureless near field scanning optical microscope probe under radial polarization illumination," *Opt. Express* **15**(7), 4106–4111 (2007).
22. T. J. Antosiewicz, P. Wróbel, and T. Szoplik, "Nanofocusing of radially polarized light with dielectric-metal-dielectric probe," *Opt. Express* **17**(11), 9191–9196 (2009).
23. D. K. Gramotnev, M. W. Vogel, and M. I. Stockman, "Optimized nonadiabatic nanofocusing of plasmons by tapered metal rod," *J. Appl. Phys.* **104**(3), 034311 (2008).
24. W. Ding, S. R. Andrews, and S. A. Maier, "Internal excitation and superfocusing of surface plasmon polaritons on a silver-coated optical fiber tip," *Phys. Rev. A* **75**(6), 063822 (2007).
25. K. Kurihara, A. Otomo, A. Syouji, J. Takahara, K. Suzuki, and S. Yokoyama, "Superfocusing modes of surface plasmon polaritons in conical geometry based on the quasi-separation of variables approach," *J. Phys. A: Math. Theor.* **40**(41), 12479–12503 (2007).
26. K. Kurihara, K. Yamamoto, J. Takahara, and A. Otomo, "Superfocusing modes of surface plasmon polaritons in a wedge-shaped geometry obtained by quasi-separation of variables," *J. Phys. A: Math. Theor.* **41**(29), 295401 (2008).
27. A. Downes, D. Salter, and A. Elfick, "Simulations of atomic resolution tip-enhanced optical microscopy," *Opt. Express* **14**(23), 11324–11329 (2006).
28. A. E. Babayan, and Kh. V. Nerkararyan, "The strong localization of surface plasmon polariton on a metal-coated tip of optical fiber," *Ultramicroscopy* **107**(12), 1136–1140 (2007).
29. J. H. Kim, and K.-B. Song, "Recent progress of nano-technology with NSOM," *Micron* **38**(4), 409–426 (2007).
30. H. J. Maas, A. Naber, H. Fuchs, U. C. Fischer, J. C. Weeber, and A. Dereux, "Imaging of photonic nanopatterns by scanning near-field optical microscopy," *J. Opt. Soc. Am. B* **19**(6), 1295–1300 (2002).
31. H. J. Maas, J. Heimel, H. Fuchs, U. C. Fischer, J. C. Weeber, and A. Dereux, "Photonic nanopatterns of gold nanostructures indicate the excitation of surface plasmon modes of a wavelength of 50–100 nm by scanning near-field optical microscopy," *J. Microsc.* **209**(Pt 3), 241–248 (2003).
32. K. Tanaka, G. W. Burr, T. Grosjean, T. Maletzky and U. C. Fischer, "Superfocussing in a metal-coated tetrahedral tip by dimensional reduction of surface-to-edge plasmon modes," *Applied Physics B: Lasers and Optics* **93**, 0946–2171 (Print) 1432–0649 (Online) (2008).
33. D. K. Gramotnev, D. F. P. Pile, M. W. Vogel, and X. Zhang, "Local electric field enhancement during nanofocusing of plasmons by a tapered gap," *Phys. Rev. B* **75**(3), 035431 (2007).
34. D. F. P. Pile, and D. K. Gramotnev, "Adiabatic and nonadiabatic nanofocusing of plasmons by tapered gap plasmon waveguides," *Appl. Phys. Lett.* **89**(4), 041111 (2006).
35. K. Tanaka, M. Tanaka, and T. Sugiyama, "Creation of strongly localized and strongly enhanced optical near-field on metallic probe-tip with surface plasmon polaritons," *Opt. Express* **14**(2), 832–846 (2006).
36. K. Tanaka, M. Tanaka, and K. Katayama, "Simulation of near-field scanning optical microscopy using a plasmonic gap probe," *Opt. Express* **14**(22), 10603–10613 (2006).
37. H. F. Frey, F. Keilmann, A. Kriele, and R. Guckenberger, "Enhancing the resolution of scanning near-field optical microscopy by a metal tip grown on an aperture probe," *Appl. Phys. Lett.* **81**(26), 5030–5032 (2002).
38. A. V. Goncharenko, H. C. Chang, and J. K. Wang, "Electric near-field enhancing properties of a finite-size metal conical nano-tip," *Ultramicroscopy* **107**(2-3), 151–157 (2007).
39. M. W. Vogel, and D. K. Gramotnev, "Optimization of plasmon nano-focusing in tapered metal rods," *J. Nanophotonics* **2**, 1–17 (2008).
40. P. Berini, "Plasmon-polariton waves guided by thin lossy metal films of finite width: Bound modes of symmetric structures," *Phys. Rev. B* **61**(15), 10484–10503 (2000).
41. A. J. Babadjanyan, N. L. Margaryan, and K. V. Nerkararyan, "Superfocusing of surface polaritons in the conical structure," *J. Appl. Phys.* **87**(8), 3785–3788 (2000).

1. Introduction

Recently, there has been great interest in the fields of nanophotonics and nano-optics [1–3] in which the construction of nanoscale optical devices is a hot subject. Recent theoretical and experimental studies have shown that optical circuits that use surface plasmon polaritons (SPPs) are promising candidates for future nanometric integrated optical circuits. For example, optical waveguides based on SPPs can be miniaturized much further than conventional, diffraction-limited optical waveguides [4–9], opening the possibility of developing nanometric integrated optical circuits.

One basic problem in this technology is how to couple incident light into metallic nanostructures. Conventional optics cannot be used to focus a laser beam into a region that is much smaller than about half the wavelength of the laser light due to the diffraction limit of light. Thus, devices are desired that are capable of effectively connecting nanodevices and waveguides without interference with other integrated elements. The most straightforward

technique is to use a nanometric aperture in a metallic screen. Several interesting apertures have been proposed that can transmit optical waves effectively with a nanoscale field distribution [10–13].

Another technique has been proposed, which is known as superfocusing or nanofocusing by SPPs. The idea originated from focusing of SPPs by a 2D wedge structure [14]. It is possible to focus a radially polarized optical SPP mode along a cylindrical metal surface by reducing the cross section of the cylinder. A practical way to achieve this is to use tapered or cone metal structures [15–26]. Such structures are used as plasmonic optical probes for near-field scanning optical microscopes (NSOMs) [27–29] and consequently they have been investigated intensively.

In most of the above-mentioned techniques for nanofocusing, a radially polarized incident beam must be employed as the incident wave. A structure that can realize nanofocusing using a linearly polarized incident wave will be useful for practical applications. Several ideas have been proposed to achieve this. A tetrahedral dielectric structure coated with a metal film that uses SPP edge modes has been suggested and this structure has been used in experimental applications [30–32]. Nanofocusing using tapered gap structures [33, 34] and a pyramidal structure on an aperture that use SPP gap modes have also been proposed [35].

However, most studies have mainly concentrated on how to obtain a highly focused and strongly enhanced optical field on a tip. The basic characteristics these focused and enhanced fields on a tip have not been sufficiently investigated. In this present paper, nanofocusing of SPPs by a pyramidal structure on an aperture is investigated using the volume integral equation (VIE) method. Nanofocusing in this structure can be achieved using a linearly polarized incident wave as the incident wave. The SPP is initially excited along the flat surface of the pyramidal structure through a rectangular aperture in a metallic screen. The excited SPP mode changes into a radially polarized mode near the tip with propagation along the pyramidal structure. It can be focused by reducing the cross section of the structure. The focusing process of SPPs on the tip of the pyramidal structure is modeled numerically. The characteristics of the focused and enhanced optical fields on the tip are investigated in detail and the dependence of the enhanced intensity on the size of the aperture is also derived.

It is not difficult to realize the structure proposed in this paper because it has a very simple structure. The basic characteristics of the focused and enhanced optical fields on the tip obtained in this paper are general and can be applied to other nanofocusing structures.

2. Geometry of the problem

The authors have investigated the basic characteristics of the plasmonic probe using the gap between two pyramidal structures on the I-shaped aperture [35, 36]. It is possible to perform the nanofocusing by the simplest version of this structure, i.e., one pyramidal structure on a rectangular aperture in the metallic screen [35]. It can be considered to be a model of “a tip on an aperture” [37].

Figure 1 shows a schematic diagram of a pyramidal structure on an aperture used in this paper. A uniform metallic screen (slab) with thickness w and complex-valued relative permittivity ε_1 is placed on the x - y plane in a vacuum whose permittivity is ε_0 . A pyramidal structure made from a metal whose complex-valued permittivity is ε_2 is fabricated on this screen and a rectangular aperture with dimensions $a_x \times a_y$ is formed in the screen (see Fig. 1). The base of the pyramidal structure has dimensions $B_x \times B_y$ and the pyramidal structure has a height h . In this paper, $B_y = a_y$ is assumed for simplicity. It is assumed that one flat surface of the pyramidal structure and one surface of the rectangular aperture are fabricated such that both surfaces lie in the y - z plane (see Fig. 1).

A Gaussian beam is assumed to be normally incident on the screen from the negative z direction below the metallic screen and the electric field polarization at $z = 0$ is assumed to be parallel to the x -axis. The beam axis lies along the z -axis. The basic characteristics of these structures will be investigated in detail in this paper.

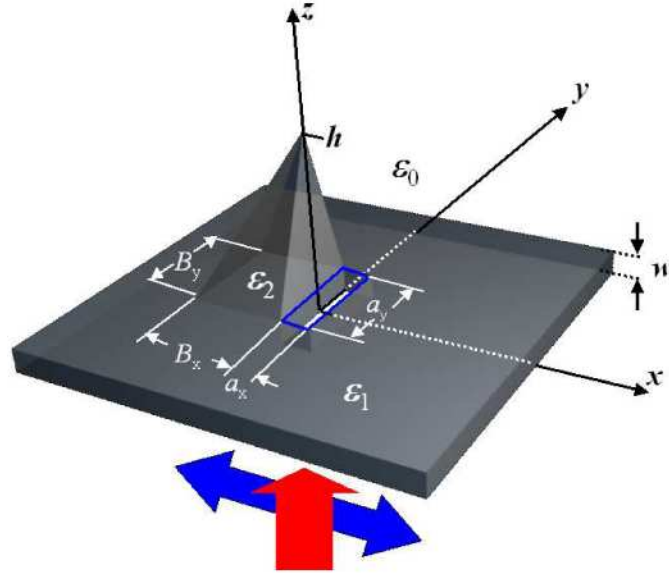


Fig. 1. Geometry of a pyramidal structure fabricated on an aperture in a metallic screen. The base of the structure has dimensions $B_x \times B_y$ and the height of the structure is h . A rectangular aperture with dimensions $a_x \times a_y$ is created in the metallic screen placed on the x - y plane. The permittivities of the surrounding free space, screen and pyramidal structure are given by ϵ_0 , ϵ_1 and ϵ_2 , respectively. A Gaussian beam (indicated by the red arrow) is normally incident on the screen from the negative z direction and its the electric field polarization at $z = 0$ (indicated by the blue arrow) is assumed to be parallel to the x -axis. The beam axis along the z -axis.

In the simulation, the wavelength is $\lambda = 633$ nm and the complex permittivities of the metallic screen and pyramidal structure are $\epsilon_1/\epsilon_0 = \epsilon_2/\epsilon_0 = -13.2 - j1.08$ (Au). The maximum amplitude of the incident electric field of the Gaussian beam is unity at $z = 0$ and its beam spot size is 2λ at $z = 0$. The screen thickness is given by $w = 90$ nm ($k_0 w = 0.9$, $k_0 = 2\pi/\lambda$). The base of the pyramidal structure has dimensions $B_x = B_y = a_y = 2155$ nm ($k_0 B_x = k_0 B_y = k_0 a_y = 21.4$) and its height is $h = 816$ nm ($k_0 h = 8.1$). The dimensions of the rectangular aperture are $a_x \times a_y = 90$ nm \times 2155 nm ($k_0 a_x \times k_0 a_y = 0.9 \times 21.4$).

3. Electric field distribution on the pyramidal structure

We solve the scattering problem shown in Fig. 1 by the VIE method [35, 36]. In this method, we first discretize the whole structure shown in Fig. 1 using tiny cubes, i.e., we consider that the pyramidal structure and the screen are composed of cubes with dimensions $\delta \times \delta \times \delta$. We then discretize the VIE by the method of moments (MoM) using rooftop functions as a basis and testing functions in each cube. Finally, we solve the resultant system of linear equations numerically. We first discretize the whole structure by cubes whose size is δ and then apply the MoM in each cube. Throughout this paper, the value of δ is given by $\delta = 10$ nm ($k_0 \delta = 0.1$).

We first solve the problem by using a cube size of δ in the discretization of the VIE by the MoM. Figures 2(a) and (b) respectively show the distributions of the main electric field component in the x - z plane (i.e., $\text{Im}[E_x(x, 0, z)]$) and those in a plane close to and parallel to the y - z plane (i.e., $\text{Im}[E_x(\delta/2, y, z)]$). Usually, the size of the cube used for the discretization of the structure is equal to that used in the application of the MoM to the VIE, as shown in this case. However, throughout this paper, we solve the problem by using a cube with a size of $\delta/2$ ($=5$ nm) when applying the MoM to the VIE, under the condition in which the whole structure is discretized by a cube of size δ . This means that each cube of δ , which makes up the whole

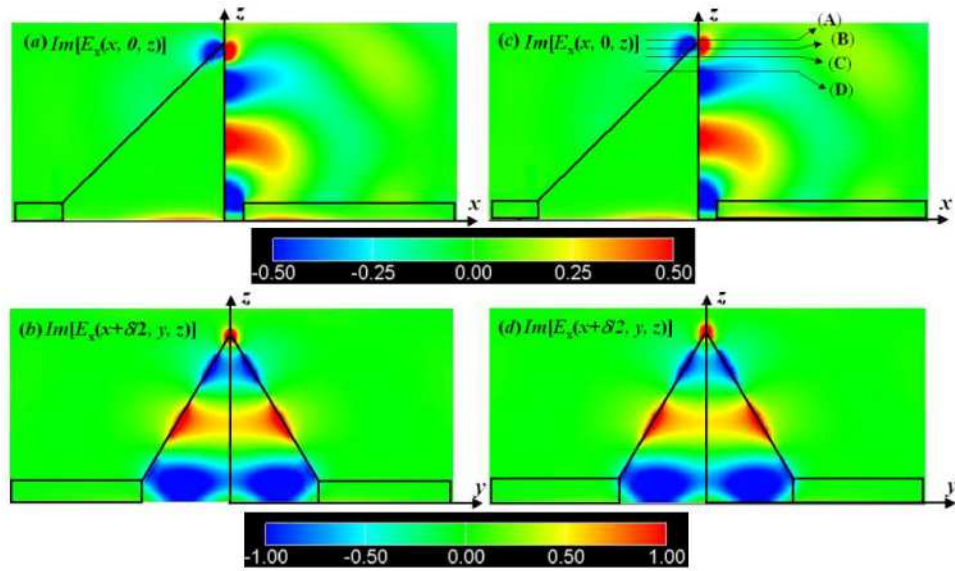


Fig. 2. Distributions of electric field component in the x - z plane $\text{Im}[E_x(x, 0, z)]$ are shown in (a) and (c), and those on a plane parallel to the y - z plane $\text{Im}[E_x(\delta/2, 0, z)]$ are shown in (b) and (d). The results of (a) and (b) are based on a discretized cube of δ (10 nm) and (c) and (d) are based on a discretized cube of $\delta/2$ in the application of MoM. In all cases, the whole structure is composed of tiny cubes of δ . The intensity is normalized by the incident intensity.

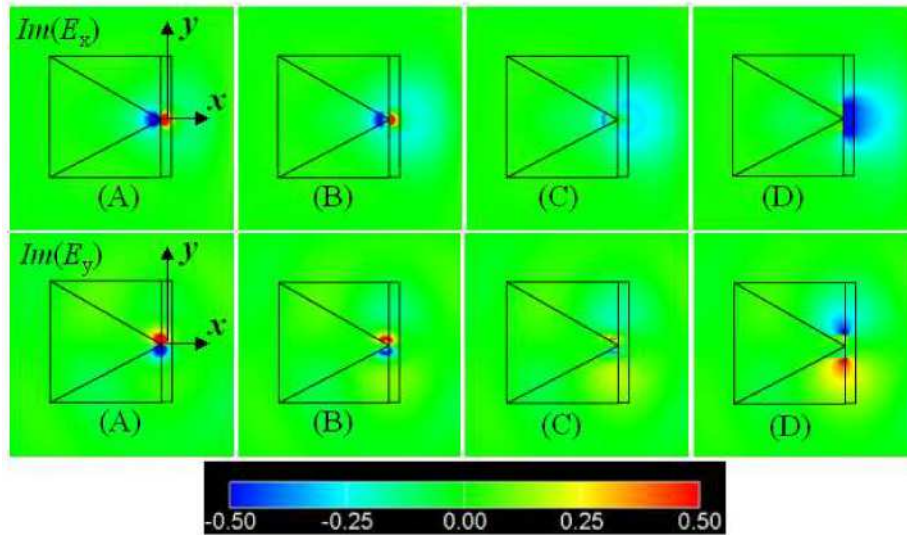


Fig. 3. Distributions of electric field component on the plane parallel to the x - y plane (i.e., $\text{Im}[E_x(x, y, \text{given})]$ and $\text{Im}[E_y(x, y, \text{given})]$). The capital letters (A)–(D) shown in the eight figures indicate the planes whose positions are illustrated in Fig. 2(c).

structure, is further subdivided into eight smaller cubes of $\delta/2$ in the numerical calculation by the MoM. The results corresponding to Figs. 2(a) and (b) in this case are shown in Figs. 2(c) and (d), respectively. Comparing the results shown in Figs. 2(a) and 2(b) with those shown in Figs. 2(c) and (d), it is apparent that the distributions in Figs. 2(a) and (b) are very similar to those in Figs. 2(c) and (d). This means that the numerical results do not depend on the size of the cube used in the MoM significantly and they demonstrate the validity of the results calculated in this paper. From the results shown in Fig. 2, it is apparent that the SPP is excited

along the flat surface on the y - z plane of the pyramidal structure through the rectangular aperture.

The excited SPP on the flat surface of the structure is focused near the tip of the structure propagation along the pyramidal structure. In order to understand the focusing process of the field with propagation, Fig. 3 shows the distributions of electric field components $\text{Im}(E_x)$ and $\text{Im}(E_y)$ in four planes. These four planes are parallel to the x - y plane and are located close to the tip of the structure (see Fig. 2(c)). The four figures in the first row of Fig. 3 show the x -component of the electric field $\text{Im}[E_x(x, y, \text{given})]$, while those in the second row show the y -component $\text{Im}[E_y(x, y, \text{given})]$. The distribution indicated by the capital letter in each figure corresponds to that in the plane whose position is shown in Fig. 2(c). The planes are located at (A) $z = h + 5$ nm, (B) $z = h - 50$ nm, (C) $z = h - 80$ nm and (D) $z = h - 125$ nm. They move from the bottom to the tip in the order (D) \rightarrow (A) and plane (A) is located just above the tip. From the numerical results shown in Figs. 2 and 3, the SPP is first mainly excited in the flat y - z plane of the pyramidal structure shown by the field in plane (D). They change to the mode whose electric field has radial components with propagation along the z -axis; i.e., with a reduction in the cross section of the structure. Notice that the x - and y -components of the field are in the counter direction among the opposite surfaces near the tip, as shown by the fields in planes (A) and (B).

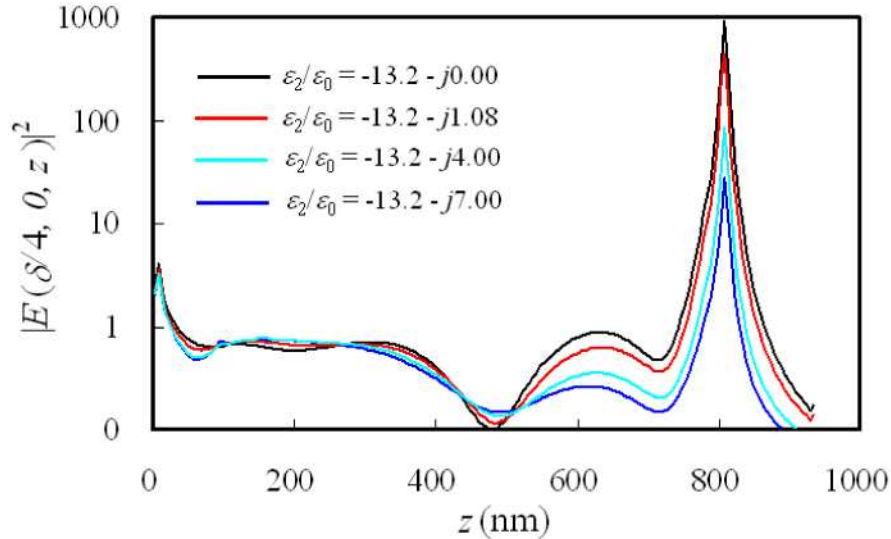


Fig. 4. Distributions of total optical intensity along the line parallel to the z -axis $|E(\delta/4, 0, z)|^2$ with the dissipation of the permittivity as a parameter. The value of $\epsilon_2/\epsilon_0 = -13.2 - j1.08$ is the real values of gold at wavelength $\lambda = 633$ nm.

Figure 4 shows typical distributions of the total optical intensity close to the y - z plane along the center line parallel to the z -axis $|E(\delta/4, 0, z)|^2$ with the dissipation of the metal of the pyramidal structure as a parameter. The maximum value is at $z = h - \delta/2$ in Fig. 4, i.e., just at the side of the cube near the tip and the x -component is the main component of the electric field. The imaginary parts of the relative permittivities given in Fig. 4 are hypothetical values except for $\epsilon_2/\epsilon_0 = -13.2 - j1.08$ which is the real relative permittivity of gold (Au). The standing wave characteristics are given by the total intensity and Fig. 4 shows that the focused and enhanced intensity is sensitive to dissipation in the metal [19].

4. Characteristics of enhanced and focused optical intensity near the tip

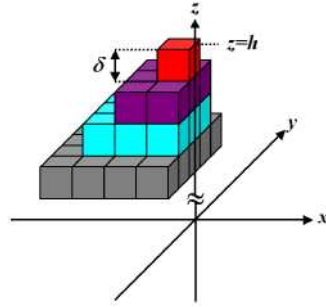


Fig. 5. Specific shapes of the four layers of the probe tip, which consists of cubes whose size is given by δ . In the numerical calculation, each cube is subdivided into eight smaller cubes whose size is $\delta/2$.

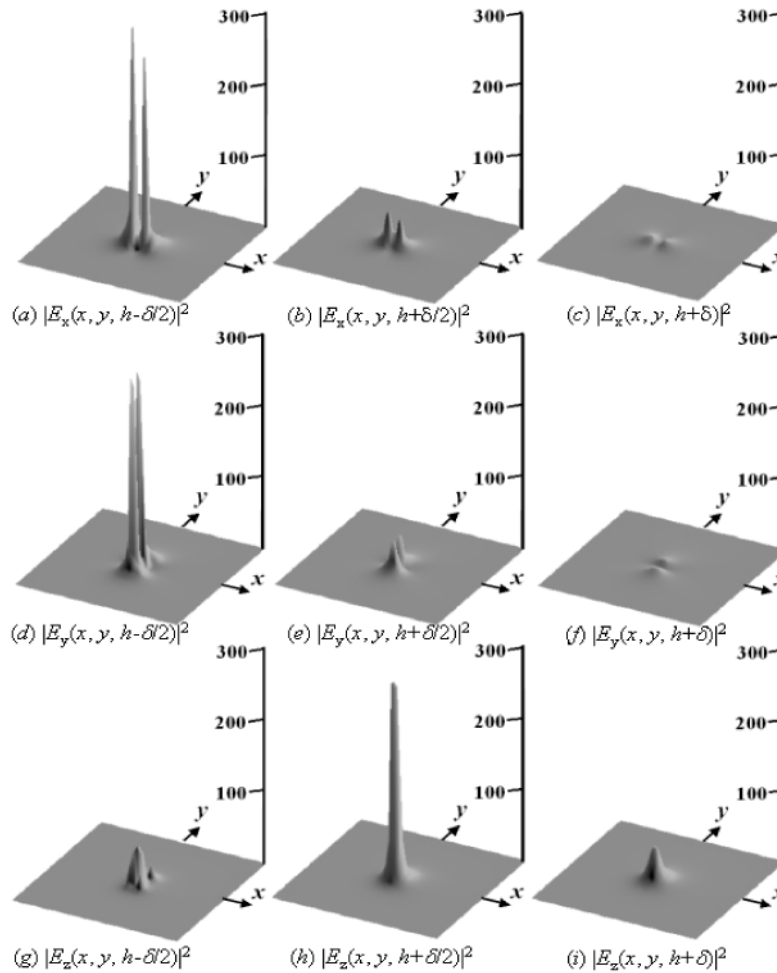


Fig. 6. Distributions of electric field components $|E_x|^2$ in (a)–(c), $|E_y|^2$ in (d)–(f) and $|E_z|^2$ in (g)–(i) in the three planes located at $z = h - \delta/2$, $z = h + \delta/2$ and $z = h + \delta$. The dimensions of the x - y plane is $200 \text{ nm} \times 200 \text{ nm}$.

Numerical calculations were performed by discretizing the whole structure by cubes with δ and by discretizing the VIE by the MoM using cubes with $\delta/2$. Figure 5 shows a specific structure near the tip by showing four layers near the tip. Each cube shown in Fig. 5 is further subdivided into eight smaller cubes in the numerical calculation. The tip is composed of one (red), six (violet), nine (blue) and twenty (gray) discretized cubes with sides of δ in each layer (see Fig. 5).

We investigate the basic characteristics of the focused and enhanced optical fields near the tip. Figure 6 shows the intensity distributions of field components $|E_x|^2$, $|E_y|^2$ and $|E_z|^2$ on the three planes located at $z = h - \delta/2$, $z = h + \delta/2$ and $z = h + \delta$ parallel to the x - y plane, i.e., intensities near the cube (the red cube in Fig. 5) on the tip. The dimensions of the x - y plane shown in Fig. 6 are $200 \text{ nm} \times 200 \text{ nm}$. In the plane at $z = h - \delta/2$, which includes the center of the cube at the tip, the maximum intensities $|E_x(x, y, h - \delta/2)|^2 \approx 287$ and $|E_y(x, y, h - \delta/2)|^2 \approx 256$ are large compared with the z -component. In the plane at $z = h + \delta/2$ just above the tip, the intensity $|E_z(x, y, h + \delta/2)|^2 \approx 257$ is large compared with other components. This indicates that the main components of the enhanced field distribution of the cube at the tip are perpendicular to the cube surface. Figure 7 shows the distribution of the focused and enhanced electric field vector $\text{Im}(\mathbf{E})$ near the tip on the plane parallel to the y - z plane ($x = -\delta/4$) and on the x - z plane. Since the enhanced field is present only near the tip (see Fig. 4), the distribution shown in Fig. 7 does not change even if the field vectors of other points are included in Fig. 7. To investigate

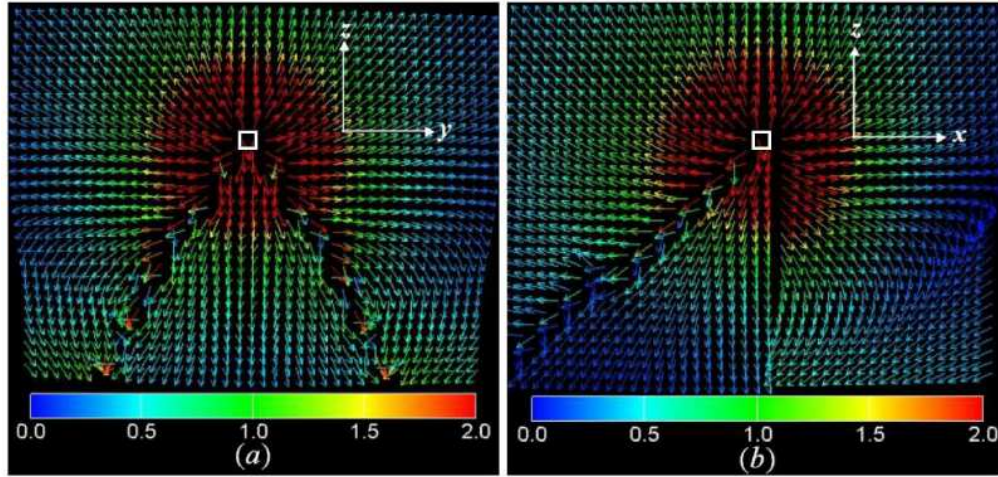


Fig. 7. Distributions of electric field vector $\text{Im}(\mathbf{E})$ near the cube on the tip whose size is given by δ (a) on the plane parallel to the y - z plane ($x = -\delta/4$) and (b) on the x - z plane. White square shows the cube on the tip. Directions of the x -, y - and z -axis are also shown.

the dependence of the focused and enhanced field shown in Fig. 7 on the distance from the tip, we consider the spherical coordinate system (R, Φ, Θ) whose origin is located at the cube center (i.e., $x = -\delta/2$, $y = 0$, $z = h - \delta/2$) on the tip shown in the inset in Fig. 8. The dependences of the intensities of radial components $|E_R|^2$ on the distance R (i.e., $R = [(x + \delta/2)^2 + y^2 + (z - h + \delta/2)^2]^{1/2}$) from the cube center for various directions are shown in Fig. 8. When the distance is larger than δ , it is possible to consider that all the field intensities that are radial components decay approximately according to R^{-3} and are similar to the approximate result of the conical structure [41]. Note that dipole local fields decay according to R^{-6} . Thus, the results in Figs. 6, 7 and 8 show that the focused and enhanced field in Fig. 7 is similar to that of a monopole whose center is located at the cube center on the tip. These results show that the tip surrounded by the enhanced fields cannot be regarded as a tiny dipole.

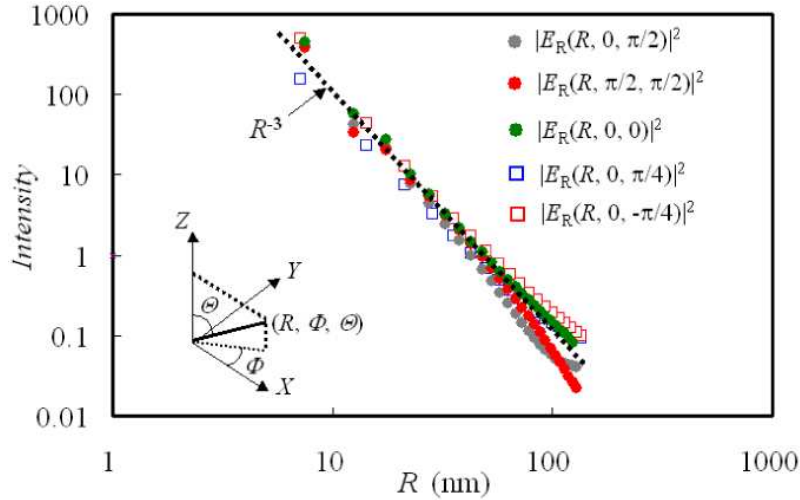
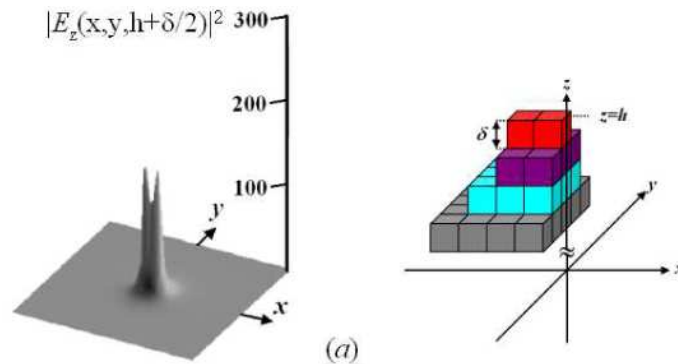


Fig. 8. Dependences of the intensity of radial component $|E_R|^2$ on the distance $R (=[(x+\delta/2)^2 + y^2 + (z-h+\delta/2)^2]^{1/2})$ in the spherical coordinate systems (R, Φ, Θ) whose origin is placed at cube center on the tip shown in the inset. The black dotted line represents the dependence R^{-3} .

5. The dependence of the field distribution on the shape of the tip

The focused and enhanced optical intensity near the tip is known to depend on the tip angle; that is, on the overall shape of the focusing structure [23]. However, only a few works have investigated the effect of the local structure of the tip on the focused field [38, 39]. The field intensity near the tip is found to be very sensitive to the shape of the tip. First, we change the original structure shown in Fig. 5 into the structure shown in Fig. 9(a) by adding an additional (red) cube to the first layer of the tip. The tip is extended in the x -direction, as illustrated in the right-hand side of Fig. 9(a). The optical intensity of the main field component just above the tip (i.e., $|E_z(x, y, h+\delta/2)|^2$), is shown in Fig. 9(a) for this case. It shows that the optical intensity is extended in the x -direction and the intensity decreases (maximum intensity ≈ 138) relative to that of the original shape shown in Fig. 5. The intensity distribution has two peaks. We next consider the case when the tip consists of three cubes extended in the y -direction, as shown in Fig. 9(b). In this case, similar results to Fig. 9(a), the intensity distribution (maximum intensity ≈ 138) is extended in the y -direction and it also has two peaks. We next consider the case when the tip consists of six cubes in the first layer, as shown in Fig. 9(c).



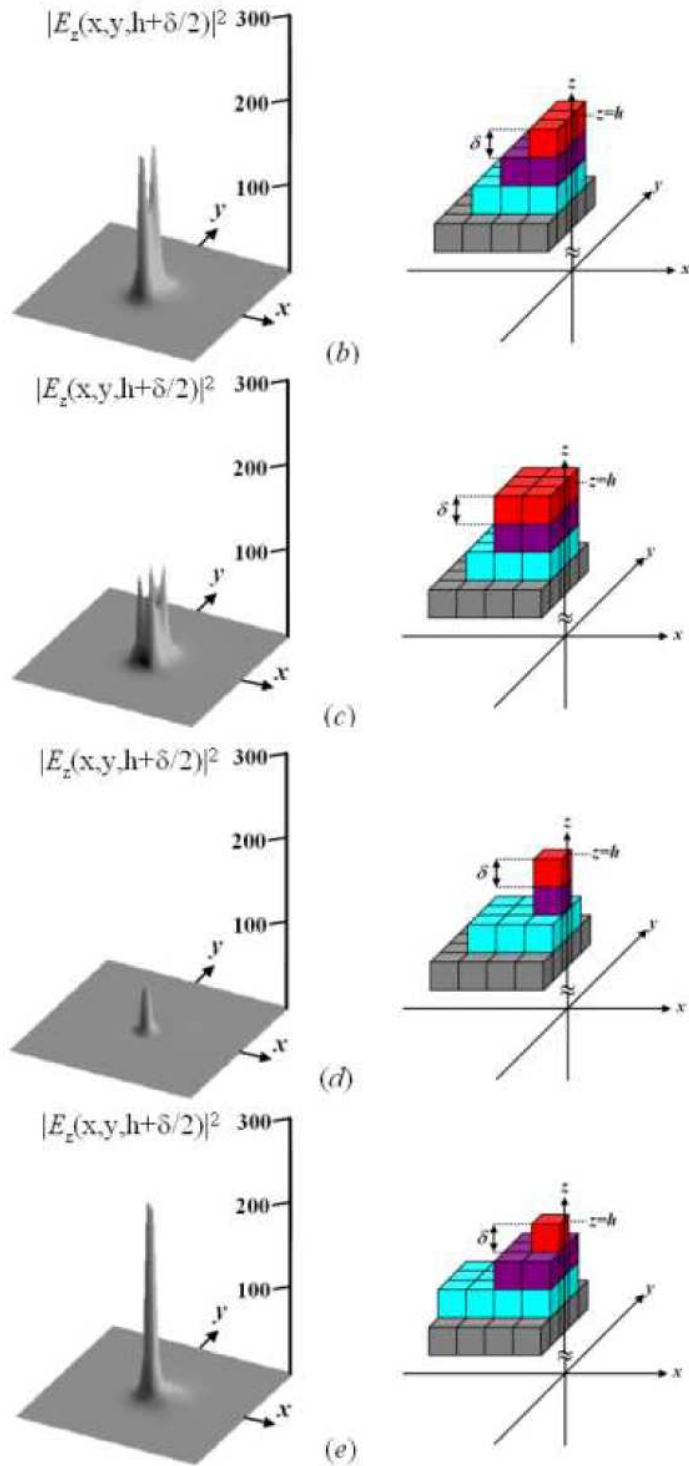


Fig. 9. Intensity distributions of the dominant electric field component just above the tip $|E_z(x, y, h + \delta/2)|^2$ for various shapes of the tip. Specific tip structures made from cubes of size δ are shown to the right of each distribution. The dimensions of the x - y plane is $200 \text{ nm} \times 200 \text{ nm}$.

In this case, there are four peaks in the intensity distribution and the intensity is smaller (maximum intensity ≈ 105) than those in Figs. 9(a) and (b). We conjecture that two and four peaks in Figs. 5(a)–(c) are due to the SPP edge mode of the cube on the tip. The intensity distributions are similar to those of SPP mode in rectangular metal stripes [40]. The results in Figs. 9(a) and (b) show the effect of polarization due to the SPP, which propagates along the flat surface of the pyramidal structure, (i.e., the x - y plane) vanishes in the intensity distribution on the tip. It is reasonable to conclude that a larger tip size generates a wider intensity distribution and a lower intensity near the tip.

We consider the case when the first and second layers both consist of a single cube, as shown in Fig. 9(d). In this case, the tip consists of two cubes in the z -direction (i.e., a sharper tip than the original shape shown in Fig. 5). Although the width of the intensity distribution is similar to that of the original shape, the intensity is much smaller (maximum intensity ≈ 50). This may be due to the large attenuation constant for a thinner SPP waveguide [40]. From the results shown in Figs. 9(a)–(d), even a small change in the structure near the tip can significantly affect the optical intensity and distribution at the tip.

Finally, we consider the case when the third layer (blue) is changed in the x -direction by adding three cubes to the original case, as shown in Fig. 9(e). This modification does not change the intensity or the distribution much (maximum intensity ≈ 245) from those of the original structure shown in Fig. 5. These results demonstrate that a small modification to the structure far from the tip does not significantly affect the field at the tip.

We now investigate the dependence of the radiation from the tip on the tip shape. Since it is possible to calculate the transmitted power W in the upper region $z > w$ in Fig. 1 [36], the normalized transmitted power W/W_0 can be calculated, where W_0 is the incident beam power. These results are given as $W/W_0 = 0.090$ for the original tip shown in Fig. 5 and $W/W_0 = 0.091, 0.089, 0.089, 0.101$, and 0.091 for Figs. 9(a)–(e), respectively. These results show that the change of the enhanced field on the tip does not significantly change the radiation from the tip.

The focusing mechanism of SPP near the tip is similar to that in other structures such as a tapered rod excited by a radially polarized incident wave. Thus, it is possible to consider that the results shown in Fig. 9 show the general nature of an SPP nanofocusing structure. Of course, these shapes do not correspond that of a practical tip. However, since it is not easy to manufacture an ideally shaped tip, these results will be useful for designing NSOMs.

6. The dependence of the maximum intensity on the aperture size

The maximum focusing and enhancement of the field on the tip created by the structure shown in Fig. 1 does not appear to be large compared with that of a tapered rod excited by a radially polarized mode [21, 23]. However, since the structure shown in Fig. 1 has many size parameters, it is not difficult to increase the maximum intensity at the tip by optimizing the tip structure. Figure 10 shows the increase in the maximum intensity just above the tip $|E_z(-\delta/2, y, h+\delta/2)|^2$ obtained by changing only the width of the rectangular aperture a_x for the normalized transmitted power W/W_0 . The maximum intensity increases with an increase in the aperture width. However, the transmitted power also increases. Since the contribution from the tip to the direct radiation from the tip is small (as shown in Sec. 3), the transmitted field will become noise when the pyramidal structure on the aperture is applied to the illumination mode of a NSOM. A larger enhanced intensity and a smaller radiated power are preferable for better characteristics for the nanofocusing structure shown in Fig. 1. Hence, optimization of the structure will be important for obtaining a high intensity at the tip and a low radiated power.

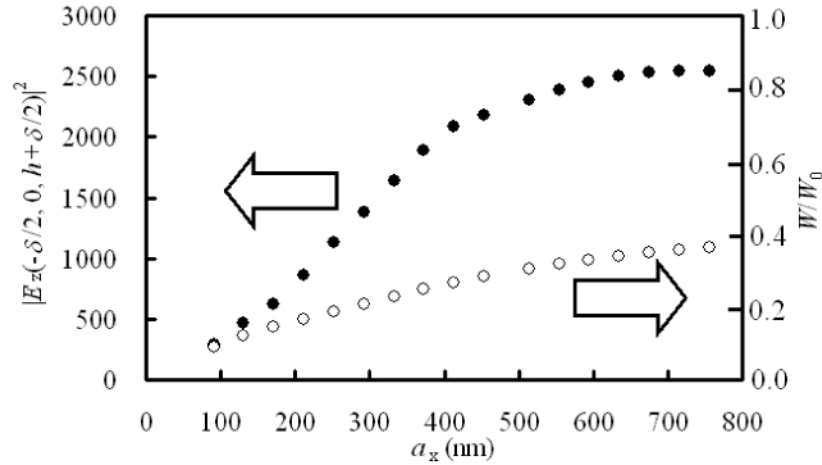


Fig. 10. Dependence of maximum intensity of the field component just above the tip $|E_z(x, y, h+\delta/2)|^2$ (solid circles) and normalized transmitted power (open circles) on the width of the rectangular aperture.

7. Conclusion

A numerical study of nanofocusing of SPPs by a pyramidal structure on a rectangular aperture is performed by the VIE method. It is shown that the nanofocusing in this structure can be performed using a linearly polarized wave as the incident wave. The characteristics of the focused and enhanced optical intensity near the tip have been investigated in detail. The focused and enhanced field near the tip is found to be similar to that of a monopole and the optical field on the tip is found to be sensitive to the local tip shape. It is also shown that the focused and enhanced intensity at the tip can be increased by increasing the width of the rectangular aperture. The limited values of the focused range size of the enhanced fields is due to limitations of our system, namely, the finite sized cubes used in the calculation. If smaller cubes are used, a smaller focusing range and higher enhanced fields can be obtained.